Environmental Science & Technology

pubs.acs.org/est

Article

Mass Budget of Methylmercury in the East Siberian Sea: The Importance of Sediment Sources

Jihee Kim, Anne L. Soerensen, Mi Seon Kim, Sangwoo Eom, Tae Siek Rhee, Young Keun Jin, and Seunghee Han*

Cite This: *Environ. Sci. Technol.* 2020, 54, 9949−9957

Read Online

ACCESS | Metrics & More | Article Recommendations | Supporting Information

ABSTRACT: Biological concentrations of methylmercury (MeHg) are elevated throughout the Arctic Ocean; however, to date, the major sources and the spatial variability of MeHg are not well quantified. To identify the major inputs and outputs of MeHg to the Arctic shelf water column, we measured MeHg concentrations in the seawater and sediment samples from the East Siberian Sea collected from August to September 2018. We found that the MeHg concentrations in seawater and pore water were higher on the slope than on the shelf, while the MeHg concentrations in the sediment were higher on the shelf than on the slope. We created a mass budget for MeHg and found that the benthic diffusion and resuspension largely exceed other sources, such as atmospheric deposition and river water input. The major sinks of MeHg in the water column were dark demethylation and evasion. When we extrapolated our findings on benthic diffusion to the entire Arctic shelf system, the annual MeHg diffusion from the shelf sediments was estimated to be 23,065 ± 939 mol yr^{-1}, about 2 times higher than previously proposed river discharges. Our study suggests that the MeHg input from shelf sediments in the Arctic Ocean is significant and has been previously underestimated.

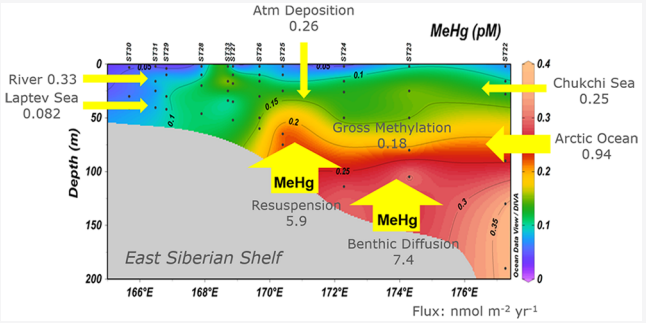

1. INTRODUCTION

Chronic exposure of humans to mercury (Hg) through seafood consumption causes harmful health effects, such as kidney damage and renal tubular disorders.[1] Therefore, Hg contamination of the Arctic marine environment is a critical human health issue, as indigenous people consume marine fish and mammals as major sources of protein.[2,3] Moreover, as climate warming decreases the sea ice coverage, commercial fisheries are emerging in the Arctic Ocean.[4] In the Arctic spring, gaseous elemental Hg [Hg(0)] carried by long-range transport from the natural and anthropogenic source is oxidized and subsequently deposited on the sea surface, thus increasing Hg concentrations in seawater.[5] The discharge of river water, snow, and ice meltwater and the Atlantic Ocean influx are also considered important Hg(II) inputs to the Arctic Ocean.[6] A recent modeling study reported that the net Hg deposition to the Arctic Ocean is 75 Mg yr^{-1}, which exceeds the riverine Hg input from the North American, Russian, and other watersheds (31−62 Mg yr^{-1}).[7]

The East Siberian Sea (ESS) is the widest shelf in the Arctic Ocean, with a surface area of 9.9×10^5 km^2 and an average depth of 58 m (Figure S1).[8] The ESS is an ecologically important zone with diverse benthic macrofauna communities, and it acts as a transition zone where eutrophic Pacific water is mixed with oligotrophic Atlantic water.[9,10] The Siberian Coastal Current flows eastward from the Laptev Sea, and along the course of the current, it is altered by cold and fresh Siberian rivers (*e.g.*, the Lena River, the Indigirka River, and the Kolyma River).[11] The Anadyr Current, which has a water mass exhibiting relatively high salinity, temperature, and nutrient-rich conditions, flows from the southeastern region of the ESS.[11,12] The eastern ESS typically shows an elevated primary productivity because of the Pacific inflow, leading to a productive epibenthic biomass.[10] The influx of Atlantic water through the eastern Fram Strait forms deep water as the Atlantic water becomes saltier, thus sinking under the less dense Arctic surface water (ASW).[13] The Atlantic deep water (ADW) then flows toward the ESS at a depth of 300−700 m.[14]

The wind from Asia can carry anthropogenic Hg to the ESS, leading to a large deposition of Hg to the sea surface.[15,16] Recent estimates of Hg deposition in the European and Russian Arctic seas (*i.e.*, Barents Sea, Kara Sea, Laptev Sea, and the ESS) showed that the largest dry deposition occurs in the ESS and that it is ascribed to the long-range transport of Hg from Asia, particularly in winter season.[16] Hg deposited to the

Received: January 8, 2020
Revised: July 13, 2020
Accepted: July 13, 2020
Published: July 14, 2020

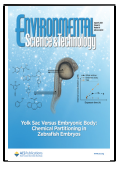

https://dx.doi.org/10.1021/acs.est.0c00154
Environ. Sci. Technol. 2020, 54, 9949−9957

ESS could be retained in marine organisms, as methylmercury (MeHg) can be produced in the subsurface water and sediment. However, the environmental factors controlling the production and transport of MeHg are not well understood in this region. The potential sources of MeHg for the ESS could be river discharge, sea ice, and snow melting, *in situ* production in the water column, and diffusive and advective transport from sediments.[17−19] A recent study on a subarctic fjord showed that active *in situ* methylation of Hg(II) occurs in stratified surface water, as river discharges of colloidal organic matter provide an anoxic microbial niche for active Hg(II) methylation.[20] The net methylation in the water column was also considered a major input of MeHg in the central Arctic Ocean and the Beaufort Sea based on the vertical profiles of MeHg, which showed peak concentrations in the subsurface layer.[21,22] The decomposition of atmospheric dimethylmercury (DMHg) followed by deposition could be an alternative source of MeHg in the ESS,[23] as shown in the mass budget for the Arctic Ocean produced by Soerensen *et al.*[6] MeHg concentrations are generally higher in ice-covered seawater than in ice-free seawater because of the limited photodemethylation of MeHg and the evasion of DMHg.[6,24]

In this study, we investigate the spatial distribution of the total Hg (THg), MeHg, and conventional hydrographic parameters in the ESS and Chukchi Sea (CS) and construct a mass budget of MeHg in the ESS water column using our field data. The ESS shelf fluxes were estimated using the MeHg concentrations in sediment pore water and overlying seawater. We then extrapolated the shelf fluxes to all Arctic shelves to produce a better-constrained estimate of the benthic diffusion in the Arctic shelves than that found in a previous study. The benthic diffusion was then compared to other sources to determine the significance of the MeHg input from the shelf sediments to the Arctic Ocean.

2. METHODS

2.1. Seawater and Sediment Sampling. Seawater and sediment sampling was conducted from August 31 to September 16, 2018 onboard the R/V Araon at 11 stations (Figure S1). A total of 55 seawater samples were taken at ST22−ST33 in the ESS, and 21 seawater samples were taken at ST01, ST04, and ST07 in the CS (Table S1). The sea ice coverage during the sampling period is shown in Figure S2. The seawater samples were collected using 10 L Niskin samplers equipped on a Rosette system (Ocean Test Equipment, Inc.). The Niskin samplers were precleaned with weak hydrochloric acid before sampling. The unfiltered seawater samples collected for Hg analysis were immediately transferred to pre-acid-cleaned 1 L Teflon bottles without headspace and preserved with 0.4% v/v hydrochloric acid. These samples were stored at 4 °C in the dark until analysis was conducted at the Gwangju Institute of Science & Technology laboratory. The leftover unfiltered water was transferred to polyethylene bottles and used for the analysis of nutrients, suspended particulate matter (SPM), and the Hg(II) methylation and MeHg demethylation incubation experiments. The method for filtering seawater for dissolved organic carbon analysis is described in Text S1 in the Supporting Information.

Sediment and pore water samples were taken at ST25, ST28, and ST31 in the expedition of 2018 and at ST13 and ST15 in that of 2019. The 2019 survey was conducted from September 10−16, 2019 onboard the R/V Araon at 12 stations. The surface sediment coring was conducted using the MUC 8 multicorer developed by Oktopus GmbH with an array of eight 80 cm polycarbonate core tubes with a diameter of 10.5 cm. After taking the cores, the surface sediments were sliced in thicknesses of 2 cm onboard. The sliced sediments were used for pore water extraction or stored in a freezer immediately. The methods for pore water collection are described in Text S1 in the Supporting Information.

2.2. Seawater Analysis. For the analysis of unfiltered THg, seawater was digested with 0.1 mL of 0.2 N bromine chloride solution for at least 12 h.[25] Following the reduction and nitrogen purging of Hg(0), the Hg(0) collected in the trap was released with thermal desorption and detected with a cold vapor atomic fluorescence spectrometer (CVAFS). The details of the THg analysis are available in Text S2 in the Supporting Information. The instrument detection limit (IDL) and the method detection limit (MDL) were 0.30 pM (n = 4) and 0.39 pM (n = 4), respectively. The method blank determined was 0.23 ± 0.067 pM (n = 4). The recovery of the matrix spike (MS) was 108 ± 12% (n = 6) and that of the certified reference material (CRM) (BCR-579, coastal seawater, EC-JRC-IRMM) was 95 ± 3.6% (n = 13). The ongoing precision was tested at every 10 samples using a calibration standard, and it was 101 ± 7.3% (n = 18). The total Hg concentrations were analyzed in duplicate, and the average relative percentage difference (RPD) was 4.9 ± 4.5% (n = 74).

The unfiltered MeHg, as the sum of monomethylmercury (MMHg) and DMHg concentrations, in seawater and pore water was measured using gas chromatography−CVAFS after distillation in the presence of 1% ammonium pyrrolidinedithiocarbamate.[26] The details of the MeHg analysis are available in Text S2 in the Supporting Information. The IDL and MDL of MeHg analysis were 8.2 fM (n = 9) and 8.8 fM (n = 9), respectively. The method blank of MeHg analysis was 43 ± 19 fM (n = 37), and the field blank MeHg concentration was 50 fM. The MS recovery was 103 ± 9.5% (n = 30) and that for CRM (IAEA 407, fish homogenate, International Atomic Energy Agency) was 99 ± 5.9% (n = 106). The ongoing precision of the standard recovery was 99.6 ± 5.4% (n = 106). Most MeHg concentrations were analyzed in duplicate, and the mean of the average RPD was 13 ± 8.2% (n = 70).

The nitrate, nitrite, and phosphate concentrations were analyzed in the Korea Polar Research Institute (KOPRI) laboratory using a gas-segmented flow system (QuAAtro, SEAL Analytical). The analytical system was calibrated using the KANSO reference material (lot no. "CF, CG, CI", KANSO Technos) before the seawater analysis.

2.3. Sediment Analysis. The frozen surface sediment samples were freeze-dried for 24 h and ground using an agate mortar and pestle. The THg concentration in the sediment was measured using atomic absorption spectroscopy (DMA-80, Milestone) based on the EPA Method 7473.[27] The details are described in Text S3 in the Supporting Information. The CRM (BCR-277R, estuarine sediment, EC-JRC-IRMM) recovery was 99 ± 4.8 (n = 4). The samples were analyzed in triplicate, and the mean relative standard deviation (RSD) was 1.8 ± 0.33% (n = 5).

MeHg in the sediment samples was analyzed following refs 28 and 29, and the details are described in Text S3 in the Supporting Information. In brief, dried sediment samples were oxidized with KBr and $CuSO_4$ solutions, and then MeHg was extracted into a dichloromethane (DCM) solution. After the extraction, MeHg in DCM was back-extracted into water and then analyzed by CVAFS. The CRM (ERM-CC580, estuarine

https://dx.doi.org/10.1021/acs.est.0c00154
Environ. Sci. Technol. 2020, 54, 9949−9957

sediment, EC-JRC-IRMM) recovery was 99 ± 12% (n = 4), and MeHg in the extraction blank was not detectable. Each sediment sample was measured in triplicate, and the mean RSD of triplicate assays was 9.1 ± 6.5% (n = 5).

The sediment carbon and nitrogen analysis methods are summarized in Text S4 in the Supporting Information. The structures of crystalline materials were analyzed using X-ray diffraction (XRD) (EmPyrean Cu LFF HR, PANalytical) at 40 kV voltage and 30 mA current. The scanning speed was 3.9° 2θ min^{-1}, and the data sampling step was 0.01° 2θ. The major compounds of sediment samples were analyzed using a X-ray fluorescence (XRF) spectrometer (PW 2404, Philips) with 60 kV current and 125 mA voltage. The sediment samples, dried at 105 °C for 3 h, were heated at 950 °C for 40 min to make glass beads for the XRF analysis.

2.4. Methylation and Demethylation Rate Constants. Dark incubation experiments were performed in the laboratory aboard the R/V Araon on September 16, 2018, using unfiltered seawater collected at ST26 (surface, 30, and 60 m) and ST29 (surface and 42 m). ^{201}Hg and ^{199}Hg were purchased from the Trace Sciences International Corporation (Canada). $CH_3{}^{199}Hg$ was synthesized as described in the established methods.[30,31] Unfiltered seawater of 3 L was injected into acid-cleaned 5 L Teflon bags using a peristaltic pump. The headspace air of the Teflon bags was removed using a peristaltic pump. Then, ^{201}Hg (128−216 pM) and Me^{199}Hg (0.85−1.10 pM) were spiked into the Teflon bags, which were then incubated at field temperature in the dark. During the incubation, sample aliquots were collected at 0, 6, 12, 18, and 25 h. The collected samples were stored in the dark after the addition of 0.4% v/v hydrochloric acid. Single incubation was performed for each water sample, and the aliquot samplings were performed in triplicate. Details of the inductively coupled plasma−mass spectroscopy analysis, calculation method, and detection limits of the Hg(II) methylation rate constant (k_m) and MeHg demethylation rate constant (k_d) are available in Text S5. The linear regression slope used to calculate k_m and k_d are shown in Figure S3.

2.5. Mass Flux Modeling of MeHg. The ESS for the mass budget estimation was defined from the Siberian coast to 139°E and 79°N for the western boundary and from the Siberian coast to 180°E and 76°N for the eastern boundary. The MeHg sources include atmospheric deposition, *in situ* Hg(II) methylation in shelf water, lateral transport with ocean currents and river discharges (including permafrost thawing), vertical diffusion and resuspension from the surface sediment, meltwater inflow, and coastal erosion.[6,8] The MeHg sinks include particle settling, photodemethylation, dark demethylation, evasion, and lateral transport with ocean currents. The details of the calculation are presented in Text S6, and the related equations and values are summarized in Tables S2 and S3. The uncertainty of each flux was estimated by the propagation of measurement or reported errors.

3. RESULTS AND DISCUSSION

3.1. Hydrographic Properties. Six different water masses were identified in the temperature−salinity diagram for the ESS and CS (Figure 1): ASW, upper halocline water (UHW), cold halocline water (CHW), lower halocline water (LHW), ADW, and Arctic Bottom Water (ABW).[32,33] The ASW, found at depths of 2−20 m in the ESS and CS, showed the lowest salinity range of 27−31, as it was affected by sea ice meltwater.[34,35] The average temperature of the ASW and

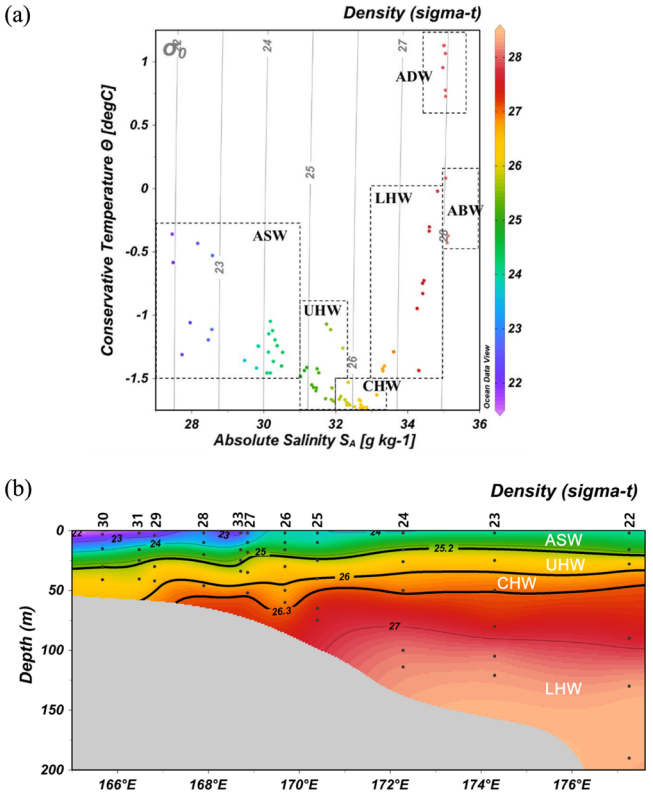

Figure 1. (a) Temperature−salinity diagram in the ESS and the CS and (b) water masses identified based on the density.[32,33] ASW: Arctic Surface Water, UHW: Upper Halocline Water, CHW: Cold Halocline Water, LHW: Lower Halocline Water, ADW: Atlantic Deep Water, and ABW: Arctic Bottom Water.

UHW was lower in the ESS than in the CS (Figure S4). The LHW showed the influence of the ADW as the temperature increased from the CHW. The CHW was found at a water depth of 50 m in the ESS and 100 m in the CS and had a mean temperature of −1.7 °C. The ADW, found at depths of 300−700 m, had a temperature range of 0.70−1.1 °C. The ABW, which originated from Greenland Sea Deep Water, was found at depths greater than 700 m and had a temperature range of −0.37−0.083 °C.[34] The DO peaks found at a depth of approximately 20 m coincided with the chlorophyll-*a* maxima, and below it were large decreases in DO by depth in the halocline depth. Fluorescence intensity was particularly high in the UHW (~30 m water depth) in the eastern ESS (ST22−24), where it is known to be influenced by nutrient-rich Pacific water advected through the Bering Strait.[10,36]

3.2. THg Distribution in the Seawater of the ESS and CS. The mean THg concentration of the ASW in the ESS was 1.0 ± 0.30 pM (Figures 2 and S5). The THg concentration range of the ASW in the ESS was lower than or similar to that reported for other Arctic shelves (Table 1). For example, the THg concentration of the Canadian Arctic Archipelago (2−5 m water depth) was 1.9 ± 2.0 pM[37] and that of the Groswater Bay (1 m water depth) near the Labrador Sea was 1.0−1.5 pM.[20] The vertical profiles of THg of the ESS showed a subsurface minimum in the lower ASW (15−20 m) and then increased with depth toward the sediments, indicating that sediment diffusion and/or particle resuspension is a significant source of THg for shelf water. The THg concentrations were commonly elevated on the surface (2−4 m) compared with those in the lower ASW, which could be caused by sea ice and

https://dx.doi.org/10.1021/acs.est.0c00154
Environ. Sci. Technol. 2020, 54, 9949−9957

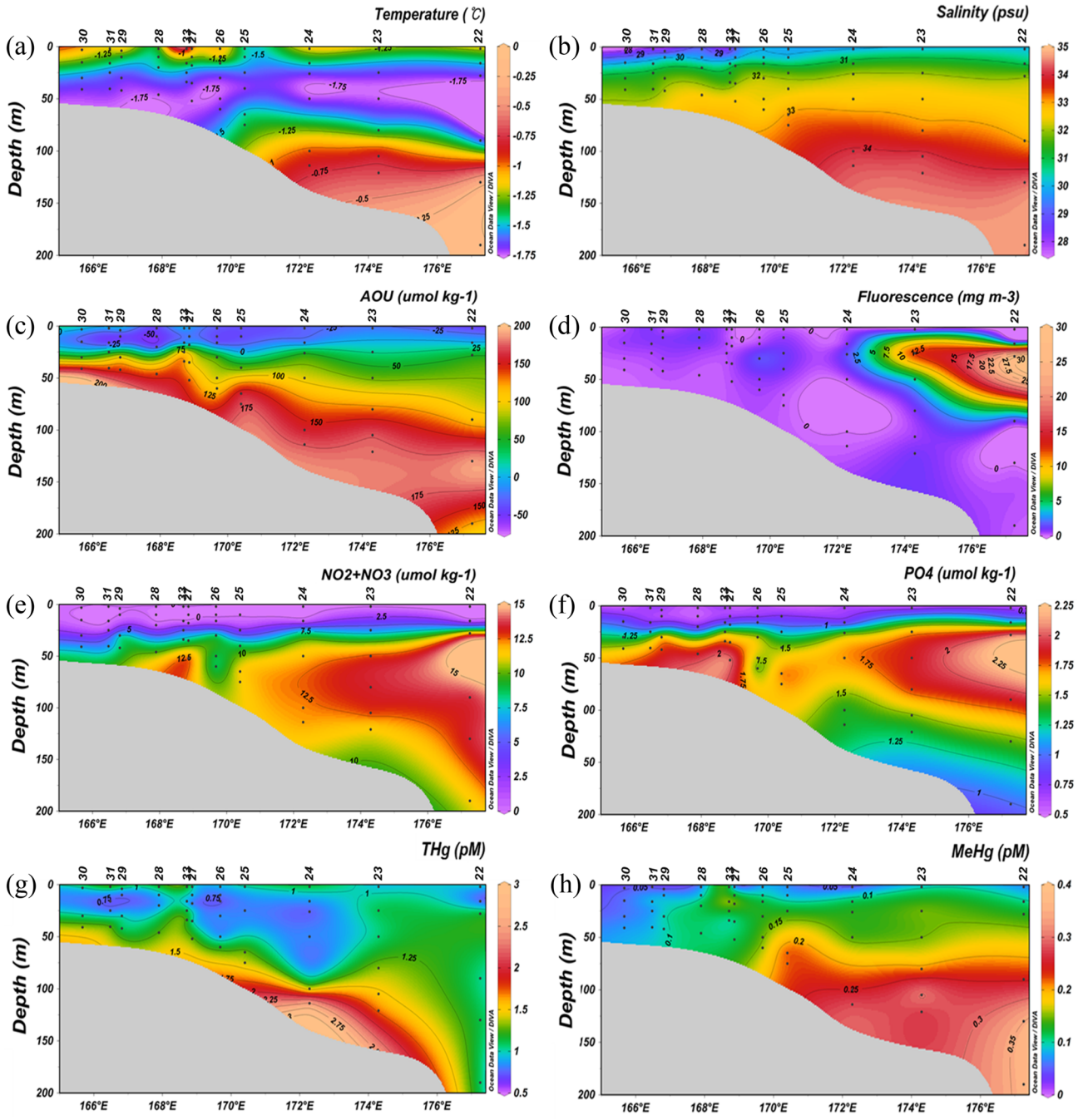

Figure 2. Distributions of hydrological properties and Hg concentrations in the ESS along a longitudinal gradient: (a) temperature, (b) salinity, (c) AOU, (d) fluorescence, (e) nitrate and nitrite, (f) phosphate, (g) THg, and (h) MeHg.

snow melt and/or atmospheric deposition. The Hg concentrations are known to be higher in sea ice and snow meltwater than in seawater. For example, the Hg concentrations in snow melt runoff in the Barrow region were 50−150 pM,[38,39] and those in snowpack meltwater in the Ny-Ålesund area were 24 ± 8.5 pM.[40] The sea ice coverage in the ESS was in fact decreasing during the sampling period (Figure S2), implying that elevated THg concentrations found in the sea surface are mainly attributable to the meltwater input as well as atmospheric deposition in the ice-free zone.

The mean THg concentration of the ASW in the CS was 1.7 ± 0.51 pM (Figure S5). The THg range of the ASW of the CS was significantly (p = 0.001, t-test) higher than that of the ESS (1.0 ± 0.30 pM, ASW) but comparable with the marginal sea of the Arctic Ocean (1.7−2.5 pM) (Table 1).[22] The higher THg levels in the CS than in the ESS could be caused by the Pacific inflow through the Bering Sea or higher meltwater and atmospheric deposition effects. According to previous cruise (SHIPPO 2014) results, the mean THg concentration in the surface seawater of the Bering Sea was 1.0 ± 0.15 pM, and thus, the Pacific inflow is not a plausible reason for the enhanced THg in the CS. The Hg(0) concentrations were 3 times higher in the seawater under contiguous ice (101 ± 98 fM) than in the ice-free seawater (32 ± 30 fM) because of the limited evasion and meltwater effects,[41,42] which explains why ASW THg is higher in the CS than in the Bering Sea. The

https://dx.doi.org/10.1021/acs.est.0c00154
Environ. Sci. Technol. 2020, 54, 9949−9957

Table 1. THg and MeHg Concentrations Found in the Arctic Seawater

	THg (pM)	MeHg (pM)	References
Baffin Bay, 20−60 m	2.4−2.6[a]	0.055[b], 0.020−0.035[c]	19
Baffin Bay, 211−216 m	1.1−1.5[a]	0.090−0.13[b], 0.14−0.19[c]	
Beaufort Sea, 33 m	1.7[a]	0.13[b], 0.23[c]	
Beaufort Sea, 125 m	1.0[a]	0.24[b], 0.36[c]	
Groswater Bay, 0−1 m	1.0 ± 0.6−1.5 ± 1.0	0.12 ± 0.058	20
Laptev Sea, 0−3000 m	0.53 ± 0.06	0.025 ± 0.030	22
Laptev Sea, 10 m	7.0		
Amusen Basin, 0−6000 m	1.3 ± 0.23	0.16 ± 0.10	
Amusen Basin, surface	2.5	0.029	
Amusen Basin, pycnocline (150 m)		0.37	
Makarov Basin, 0−3500 m	1.0 ± 0.25	0.21 ± 0.080	
Makarov Basin, surface	1.7	0.034	
Makarov Basin, pycnocline (200 m)		0.34	
Canadian Arctic Archipelago, 2−5 m	1.9 ± 2.0	0.12 ± 0.046[b]	37
Hudson Bay, 2−5 m	2.1 ± 2.6	0.12 ± 0.055[b]	
Chukchi Shelf, <200 m	1.1 ± 0.60[d]	0.028 ± 0.007[b,d]	44
Western Arctic Ocean (Bering Sea, Bering Strait, Makarov Basin, Eurasian Basin, and Canada Basin), 0−50 m	0.41−2.9[d]	0.064 ± 0.065[b,d]	
Canada Basin, Beaufort Sea, and Western CAA, 0−500 m	1.9 ± 1.3	0.30 ± 0.14	57
Eastern CAA and Baffin Bay, 0−500 m	2.6 ± 2.1	0.19 ± 0.08	
Labrador Sea, 0−500 m	0.62 ± 0.19	0.090 ± 0.040	
ESS, ASW, 0−20 m	1.0 ± 0.30	0.089 ± 0.033	this study
ESS, UHW, 20−45 m	1.0 ± 0.23	0.11 ± 0.028	
ESS, CHW, 45−60 m	1.1 ± 0.21	0.14 ± 0.019	
ESS, LHW, >60 m	1.4 ± 0.52	0.27 ± 0.058	
CS, ASW, 0−20 m	1.7 ± 0.51	0.14 ± 0.071	
CS, UHW, 20−50 m	1.0 ± 0.20	0.33 ± 0.11	
CS, CHW, 50−150 m	0.87 ± 0.21	0.20 ± 0.10	
CS, LHW, 150−300 m	0.82 ± 0.32	0.25 ± 0.11	
CS, ADW, 300−700 m	0.74 ± 0.073	0.28 ± 0.043	
CS, ABW, > 700 m	0.82 ± 0.10	0.24 ± 0.021	

[a]Inorganic mercury. [b]Monomethylmercury. [c]Dimethylmercury. [d]Filtered water.

meltwater contribution of THg concentrations could be larger in the CS than in the ESS, as the sea ice melt area was larger in the CS than in the ESS during the sampling period (Figure S2). In support of this, the decrease of salinity in surface seawater was more severe in the CS (27.3−27.5 at ST01, 04, and 07) than in the ESS (29.3−30.1 at ST 22−28). While there was no significant ($p > 0.01$) correlation between THg and salinity (and density) in the ESS, strong negative correlations were found between THg and salinity ($r = -0.82$, $p < 0.01$) and between THg and density ($r = -0.83$, $p < 0.01$) in the CS (Table S4). The reverse distribution pattern of THg to salinity (and density) is attributed to the scavenged type distribution, in which Hg concentrations rapidly decrease by depth following the particle distribution pattern.[43]

3.3. MeHg Distribution in the Seawater of the ESS and CS. The mean MeHg concentration of the ASW in the ESS was 0.089 ± 0.033 pM (Figure 2 and S5). The ASW MeHg concentration was slightly lower than that in the Beaufort Sea (0.13 pM, 33 m),[19] the Canadian Arctic Archipelago (0.12 ± 0.046 pM, 2−5 m),[37] and the Hudson Bay (0.12 ± 0.055 pM, 2−5 m; Table 1).[37] We found significantly positive correlations of MeHg with salinity ($r = 0.81$, $p < 0.01$) and density ($r = 0.80$, $p < 0.01$) (Table S4) as MeHg concentrations typically increased in the LHW with increasing salinity, indicating that sediment resuspension or benthic diffusion could be important. This also explains the significant correlation ($r = 0.64$, $p < 0.01$) found between MeHg and AOU in the Pearson's matrix. Several MeHg profiles on the interior shelf (ST27, ST28, and ST31) showed subsurface peak concentrations at depths of approximately 20 m, consistent with the fluorescence maxima.

The mean MeHg concentration in the ASW of the CS was 0.14 ± 0.071 pM (Figure S5). The MeHg concentration in the ASW of the CS was significantly ($p = 0.032$, t-test) higher than that of the ESS (0.089 ± 0.033 pM) and western Arctic Ocean (0.064 ± 0.065 pM, 0−51 m; Table 1).[44] However, it is similar to that found on the surface of the Canadian Arctic Archipelago and Hudson Bay (approximately 0.12 pM at a 2−5 m water depth). The MeHg subsurface maximum in the CS was found in the UHW at depths of 35−45 m (0.30−0.43 pM) in relation to the fluorescence maxima found at the same depth. The depths of the fluorescence maxima were consistently shallower than the nutrient peak depths (100−150 m) in the CS, with quite low nutrient concentrations within the fluorescence maxima (Figure S6). The deep chlorophyll maxima are typical features of the Arctic Ocean in summer after the bloom period.[45] The tight link between the fluorescence maxima and the MeHg peak depths could be explained by two reasons: (1) as MeHg was measured in unfiltered seawater, the accumulation of phytoplankton at the deep chlorophyll maxima could lead to high concentrations of phytoplankton-associated MeHg or (2) high-quality organic matter led to the increased *in situ* methylation at the fluorescence maxima depth. The latter is more suitable to

https://dx.doi.org/10.1021/acs.est.0c00154
Environ. Sci. Technol. 2020, 54, 9949−9957

explain enhanced MeHg at the fluorescence maxima based on the previous studies.[21,22] Nonetheless, high-resolution k_m measurements in the water column of CS are needed to clarify this explanation.

3.4. THg and MeHg in the ESS Sediment. The sediment THg concentrations on the shelf (<100 m) were 55 ± 1 ng g^{-1} at ST31, 61 ± 1 ng g^{-1} at ST28, and 73 ± 1 ng g^{-1} at ST25 (Figure 3 and Table S5). The THg concentrations, increasing

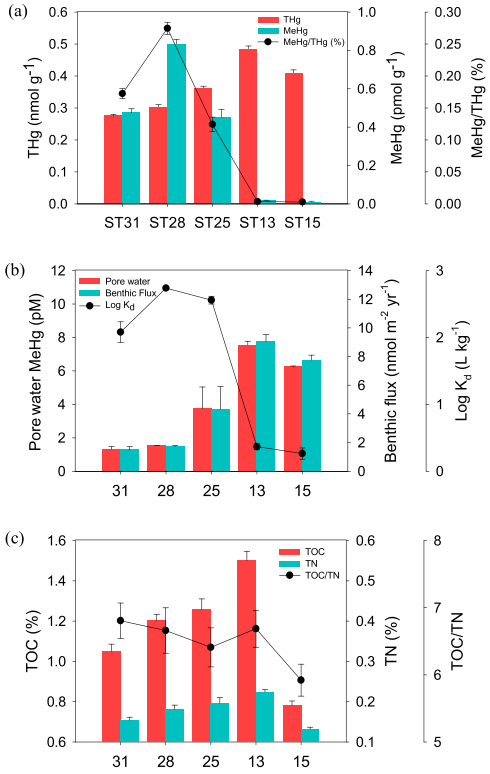

Figure 3. Variations of (a) sediment THg, MeHg, and MeHg-to-total Hg ratio; (b) pore water MeHg, particle-water partition coefficient (K_d) of MeHg and benthic flux of MeHg; and (c) sediment TOC, TN, and TOC-to-TN ratio of the ESS.

toward the slope (100−500 m), were 97 ± 2 ng g^{-1} at ST13 and 82 ± 2 ng g^{-1} at ST15. The shelf THg concentrations were comparable with those in the marginal sea of the Arctic Ocean (*e.g.*, Beaufort Sea 41 ± 29 ng g^{-1}; CS 31 ± 10 ng g^{-1}), and the slope THg concentrations were similar to those found in the Arctic Ocean Basin (82 ± 26 ng g^{-1}).[46] A positive correlation between THg and total organic carbon (TOC) was found except at ST15. In fact, the distinctively autochthonous characteristics of TOC, represented by a lower TOC/TN ratio than other sites, were found at the slope site of ST15 (Figure 3c).

The sediment MeHg concentrations at the shelf sites were 100 ± 4 pg g^{-1} at ST31, 168 ± 5 pg g^{-1} at ST28, and 91 ± 8 pg g^{-1} at ST25 (Figure 3 and Table S5). The MeHg concentrations at the slope sites were 3.5 ± 0.4 pg g^{-1} at ST13 and 2.3 ± 0.4 pg g^{-1} at ST15, which were lower than those in the shelf. The MeHg production rates of the shelf and slope sediments are regulated by the availability of soluble Hg(II) or the activity of Hg(II) methylating microbes, related to sediment organic matter and redox conditions.[47] Based on the solubility of MeHg, we expect the solubility of Hg(II) to be higher at the slope than the shelf sites (Figure 3b), then the microbial activities might be more favorable for Hg(II) methylation on the shelf than the slope. In fact, the quality of organic matter was more autochthonous on the slope than the shelf based on the TOC/TN ratio, and thus, it cannot provide suitable explanation for the higher MeHg on the shelf. The color of the top 2 cm sediment of ST15 was light brown, representing ferric iron (*e.g.*, FeOOH), while that of ST28 and ST31 was olive-gray, indicating the presence of ferrous iron (*e.g.*, FeS) produced under anaerobic condition (Figure S7).[48] Because Hg(II) methylating microbes are strictly anaerobic based on the Hg(II)-methylating gene, *hgcAB*, survey,[49] active methylation is not expected on the slope despite the presence of reactive organic matter.

The spatial gradient of the MeHg concentration in pore water was opposite to that of sediment MeHg, and the concentration was significantly higher at the slope sites than at the shelf sites (Figure 3). This trend led to the higher particle−water partition coefficients (k_d) of MeHg on the shelf sites than on the slope sites. As neither TOC nor C/N ratios provided plausible causes for the largely decreased k_d of MeHg at ST13 to ST15, the solubility trend could be related to the distinct mineral composition or sediment redox condition between the shelf and slope. In the mineral and elemental composition tests using the XRD and XRF, respectively, comparable compositions were found between the shelf and slope, except the slightly increased manganese oxide and feldspar contents, and decreased kaolinite content on the slope sites, eliminating the former possibility (Figure S8; Tables S6 and S7). The formation of acid-volatile sulfide (AVS), mainly mackinawite, greigite, and elemental sulfur, in the interior shelf sites could describe the largely decreased solubility of MeHg at the shelf sites. The pore water solubilities of Hg and MeHg were largely controlled by AVS in the low TOC sediments (<2%) and by TOC in the high TOC sediments of the temperate shelf.[47] The sediment core images support our suggestion as gray colors representing that AVS are typical in the shelf cores, while light brown colors representing FeOOH are shown in the slope cores (Figure S7).

3.5. Sources and Sinks of MeHg in the ESS. In the MeHg mass budgets, the lateral inputs of MeHg through ocean currents were estimated as 0.94 nmol m^{-2} yr^{-1} for the Arctic Ocean, 0.25 ± 0.062 nmol m^{-2} yr^{-1} for the CS, and 0.082 ± 0.098 nmol m^{-2} yr^{-1} for the Laptev Sea (Figure 4 and Table S2). The MeHg inputs through river discharge were less than the Arctic influx, as they were 0.23 nmol m^{-2} yr^{-1} for the Kolyma River and 0.093 nmol m^{-2} yr^{-1} for the Indigirka River. The MeHg influxes through meltwater were comparable to the river flux: 0.28 ± 0.12 nmol m^{-2} yr^{-1} for melt pond, 0.27 ± 0.15 nmol m^{-2} yr^{-1} for sea ice, and 0.076 ± 0.036 nmol m^{-2} yr^{-1} for snow. The coastal erosion of MeHg was estimated to be 0.28 nmol m^{-2} yr^{-1} based on the erosion flux of THg and the fraction of eroded THg found as MeHg.

The wet and dry deposition of MeHg was estimated as 0.26 ± 0.31 nmol m^{-2} yr^{-1} (Figure 4 and Table S2). Our value is less than the wet deposition (0.55 nmol m^{-2} yr^{-1}) estimated in the Canadian Arctic Archipelago[23] and overall Arctic Ocean (3.6 nmol m^{-2} yr^{-1}).[6] The wet deposition of MeHg, estimated using the MeHg concentration of rainwater collected from the Arctic Ocean[6] and the wet precipitation depth measured in Wrangel Island in 2018 (139 mm yr^{-1}), was 0.070 nmol m^{-2} yr^{-1} that is reasonably lower than the total deposition flux.

The gross dark Hg(II) methylation flux was estimated as 0.18 ± 0.089 nmol m^{-2} yr^{-1} based on the dark k_m values

https://dx.doi.org/10.1021/acs.est.0c00154
Environ. Sci. Technol. 2020, 54, 9949−9957

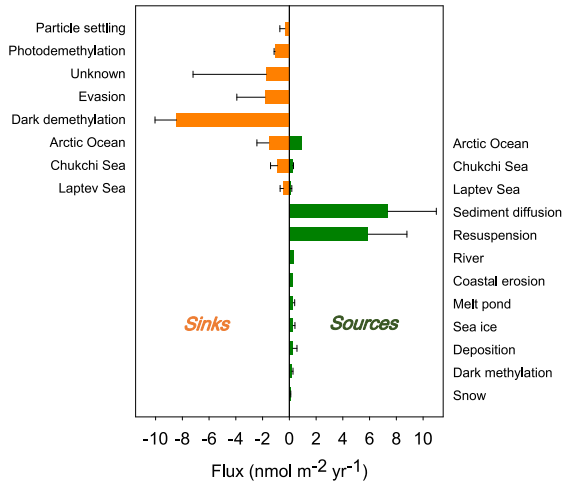

Figure 4. MeHg source (green) and sink (orange) budget in the ESS. The fluxes, equations, and used parameters are summarized in Tables S2 and S3 in the Supporting Information.

summarized in Table S8. The dark k_m levels measured in the ST26 and ST29 of the ESS seawater ranged from 1.0×10^{-5} to 5.0×10^{-5} day^{-1}, with a mean value of $2.5 \times 10^{-5} \pm 1.5 \times 10^{-5}$ day^{-1}. These rate constants are lower than those found in other marine studies performed in the Arctic zone.[19,50] The dark k_d levels, ranging from 5.6×10^{-3} to 1.1×10^{-2} day^{-1} with a mean of $7.7 \times 10^{-3} \pm 2.0 \times 10^{-3}$ day^{-1}, are also lower than those found in the Canadian Archipelago.[19,50] In our study, the dark k_m levels were higher in the halocline (UHW and CHW) water than those in the ASW and were higher at the site close to the slope.

The mean sediment diffusion was 7.4 ± 3.6 nmol m^{-2} yr^{-1}, and the flux was higher on the slope (ST13 and ST15) than on the shelf (ST28 and ST31), as predicted from the MeHg concentrations in pore water. Our mean benthic diffusion was 1 order of magnitude higher than that of Lake Melville connected to the Labrador Sea (0.33 nmol m^{-2} yr^{-1})[20] and the Arctic Ocean (0.33 nmol m^{-2} yr^{-1})[6] but was comparable with the temperate continental shelf (3.3 nmol m^{-2} yr^{-1}).[51] The resuspension of MeHg was estimated to be 5.9 ± 2.9 nmol m^{-2} yr^{-1} using the ratio (1.3; Table S2) between diffusion and resuspension.[20,52] Overall, the benthic diffusion and resuspension largely exceed other sources, such as atmospheric deposition, lateral transport, and gross Hg(II) methylation in the water column. Nonetheless, note that our result could be specific to the shelf zone, as *in situ* water column methylation has been suggested to be a major MeHg input for the deeper zones of the Arctic Ocean.[21,22]

The sinks of MeHg include particle settling, photodemethylation, dark demethylation, evasion, and lateral transport (Figure 4 and Table S3). The MeHg removal through particle settling was estimated as 0.33 ± 0.38 nmol m^{-2} yr^{-1}. This value is comparable to that of the Arctic Ocean (0.58 nmol m^{-2} yr^{-1}), but less than that of the Arctic lake (2.3 nmol m^{-2} yr^{-1}), where higher SPM concentrations lead to higher settling flux than the Arctic Ocean. The evasion of MeHg was estimated to be 1.8 ± 2.1 nmol m^{-2} yr^{-1}, and the loss of MeHg through photodemethylation and dark demethylation was calculated to be 1.1 ± 0.075 and 8.4 ± 1.6 nmol m^{-2} yr^{-1}, respectively. The outputs of MeHg through lateral transports were 1.5 ± 0.90 nmol m^{-2} yr^{-1} for the Arctic Ocean, 0.88 ± 0.52 nmol m^{-2} yr^{-1} for the CS, and 0.43 ± 0.25 nmol m^{-2} yr^{-1} for the Laptev Sea. The unknown sink(1.7 ± 5.5 nmol m^{-2} yr^{-1}) was approximated by the imbalance of the MeHg mass budget. Overall, the largest sink of MeHg in the ESS was through water column demethylation, consistent with the literature results.[6,20]

The mass budgets of this study have certain caveats related to the restricted experimental methods and limited sampling seasons and sites. A relatively small number of samples were collected on the offshore sites of the eastern ESS to generate a MeHg mass budget for the entire ESS, which may lead to limited spatial representativeness. The diffusion of MeHg estimated using the pore water and overlying water concentrations may underestimate the actual sediment flux.[53] For example, a study in the temperate coastal sites found that the diffusion flux of MeHg, determined using flux chambers, was 2−4 times higher than the flux estimated by the core method.[53] The resuspension can be another major uncertainty in our budget, as the ratio between diffusion and resuspension would be site-specific. Regarding the temporal restriction, the erosion and diffusion flux can be variable by the seasonal dynamics of pore water MeHg, which could be higher in September than in other months as the peak primary production of ESS was reported in September.[54] Despite these limitations, we suggest that the sediment transport is a major source of MeHg in the ESS water column based on its overwhelming flux.

4. ENVIRONMENTAL IMPLICATIONS

The Arctic Ocean has unique characteristics, as its continental shelf accounts for nearly half (approximately 53%) of its total surface area.[55,56] The Arctic Ocean shelves can be divided into the easy shelf zone and the steep slope zone. Following this categorization, we estimated the overall sediment diffusion flux of MeHg (Table S9), assuming that the MeHg sediment fluxes in the shelf zone were similar to what we estimated for ST28 and ST31 and those in the slope zone were similar to what we estimated for ST13 and ST15. The benthic flux of MeHg from the overall shelf sediments was estimated as 23,065 ± 939 mol yr^{-1}. This value largely exceeds the river discharge (12,500 mol yr^{-1}), coastal erosion (7480 mol yr^{-1}), Pacific and Atlantic inputs (7000 mol yr^{-1}), and meltwater flux (2490 mol yr^{-1}) in the Arctic Ocean.[6] However, it was lower than the net Hg(II) methylation in the water column (49,800 mol yr^{-1}) and the atmospheric deposition (39,900 mol yr^{-1}).[6] Thus, we found that the input from the shelf sediments was the second most important "external" source of MeHg to the Arctic Ocean. Nonetheless, more data collection is necessary to confirm our conclusion, as the inputs and outputs of MeHg are changeable by season and climate.

■ ASSOCIATED CONTENT

Supporting Information

The Supporting Information is available free of charge at https://pubs.acs.org/doi/10.1021/acs.est.0c00154.

Seawater filtration and sediment pore water collection, seawater THg and MeHg analysis, sediment THg and MeHg analysis, measurements of sediment carbon and nitrogen, Hg(II) methylation rate constant (k_m) and MeHg demethylation rate constant (k_d), mass flux modeling of MeHg, water depth and GPS information, MeHg source budget, MeHg sink budget, Person's correlation matrix, sediment concentrations, major

https://dx.doi.org/10.1021/acs.est.0c00154
Environ. Sci. Technol. 2020, 54, 9949−9957

compound composition, major mineral composition, dark methylation rate constants and dark demethylation rate constants, benthic fluxes of MeHg estimation, locations of the sampling sites and major ocean currents, sea ice concentrations, kinetic models, vertical profiles, vertical distributions, images of the sediment cores collected, XRD diffractograms, and sample collection sites (PDF)

AUTHOR INFORMATION

Corresponding Author

Seunghee Han − *School of Earth Sciences and Environmental Engineering, Gwangju Institute of Science and Technology (GIST), Gwangju 61005, Republic of Korea;* orcid.org/0000-0002-3284-0106; Phone: 82-62-715-2438; Email: shan@gist.ac.kr; Fax: 82-62-715-2434

Authors

Jihee Kim − *School of Earth Sciences and Environmental Engineering, Gwangju Institute of Science and Technology (GIST), Gwangju 61005, Republic of Korea*

Anne L. Soerensen − *Department of Environmental Research and Monitoring, Swedish Museum of Natural History, Stockholm 114 18, Sweden;* orcid.org/0000-0002-8490-8600

Mi Seon Kim − *Department of Ocean Environmental Sciences, Chungnam National University, Daejeon 34134, Republic of Korea; Division of Polar Ocean Sciences, Korea Polar Research Institute, Incheon 21990, Republic of Korea*

Sangwoo Eom − *School of Earth Sciences and Environmental Engineering, Gwangju Institute of Science and Technology (GIST), Gwangju 61005, Republic of Korea*

Tae Siek Rhee − *Division of Polar Ocean Sciences, Korea Polar Research Institute, Incheon 21990, Republic of Korea*

Young Keun Jin − *Division of Polar Earth System Sciences, Korea Polar Research Institute, Incheon 21990, Republic of Korea*

Complete contact information is available at: https://pubs.acs.org/10.1021/acs.est.0c00154

Notes

The authors declare no competing financial interest.

ACKNOWLEDGMENTS

This study was supported by the Polar Academic Program (PE18900) of the Korea Polar Research Institute and the AMAGE program (KIMST no. 20160247) funded by the Ministry of Oceans and Fisheries, Korea.

REFERENCES

(1) Mergler, D.; Anderson, H. A.; Chan, L. H. M.; Mahaffey, K. R.; Murray, M.; Sakamoto, M.; Stern, A. H. Methylmercury Exposure and Health Effects in Humans: A Worldwide Concern. *Ambio* **2007**, *36*, 3−11.

(2) Sundseth, K.; Pacyna, J.; Banel, A.; Pacyna, E.; Rautio, A. Climate Change Impacts on Environmental and Human Exposure to Mercury in the Arctic. *Int. J. Environ. Res. Public Health* **2015**, *12*, 3579−3599.

(3) Walker, J. B.; Houseman, J.; Seddon, L.; McMullen, E.; Tofflemire, K.; Mills, C.; Corriveau, A.; Weber, J.-P.; LeBlanc, A.; Walker, M.; Donaldson, S. G.; Van Oostdam, J. Maternal and umbilical cord blood levels of mercury, lead, cadmium, and essential trace elements in Arctic Canada. *Environ. Res.* **2006**, *100*, 295−318.

(4) Christiansen, J. S.; Mecklenburg, C. W.; Karamushko, O. V. Arctic marine fishes and their fisheries in light of global change. *Global Change Biol.* **2014**, *20*, 352−359.

(5) Kirk, J. L.; Lehnherr, I.; Andersson, M.; Braune, B. M.; Chan, L.; Dastoor, A. P.; Durnford, D.; Gleason, A. L.; Loseto, L. L.; Steffen, A.; St Louis, V. L. Mercury in Arctic marine ecosystems: Sources, pathways and exposure. *Environ. Res.* **2012**, *119*, 64−87.

(6) Soerensen, A. L.; Jacob, D. J.; Schartup, A. T.; Fisher, J. A.; Lehnherr, I.; St Louis, V. L.; Heimbürger, L.-E.; Sonke, J. E.; Krabbenhoft, D. P.; Sunderland, E. M. A mass budget for mercury and methylmercury in the Arctic Ocean. *Global Biogeochem. Cycles* **2016**, *30*, 560−575.

(7) Dastoor, A.; Ryzhkov, A.; Durnford, D.; Lehnherr, I.; Steffen, A.; Morrison, H. Atmospheric mercury in the Canadian Arctic. Part II: Insight from modeling. *Sci. Total Environ.* **2015**, *509*−*510*, 16−27.

(8) Outridge, P. M.; Macdonald, R. W.; Wang, F.; Stern, G. A.; Dastoor, A. P. A mass balance inventory of mercury in the Arctic Ocean. *Environ. Chem.* **2008**, *5*, 89−111.

(9) Anderson, L. G.; Björk, G.; Jutterström, S.; Pipko, I.; Shakhova, N.; Semiletov, I.; WaÅhlström, I. East Siberian Sea, an Arctic region of very high biogeochemical activity. *Biogeosciences* **2011**, *8*, 1745−1754.

(10) Grebmeier, J. M.; Overland, J. E.; Moore, S. E.; Farley, E. V.; Carmack, E. C.; Cooper, L. W.; Frey, K. E.; Helle, J. H.; McLaughlin, F. A.; McNutt, S. L. A major ecosystem shift in the northern Bering sea. *Science* **2006**, *311*, 1461−1464.

(11) Pisareva, M. N.; Pickart, R. S.; Spall, M. A.; Nobre, C.; Torres, D. J.; Moore, G. W. K.; Whitledge, T. E. Flow of pacific water in the western Chukchi Sea: Results from the 2009 RUSALCA expedition. *Deep Sea Res., Part I* **2015**, *105*, 53−73.

(12) Mathis, J. T.; Pickart, R. S.; Hansell, D. A.; Kadko, D.; Bates, N. R. Eddy transport of organic carbon and nutrients from the Chukchi Shelf: Impact on the upper halocline of the western Arctic Ocean. *J. Geophys. Res.: Oceans* **2007**, *112*, C05011.

(13) Jones, E. P. Circulation in the Arctic Ocean. *Ocean Polar Res.* **2001**, *20*, 139−146.

(14) Ikeda, M.; Tanaka, S. S.; Watanabe, Y. W. Circulation patterns in the lower Arctic Ocean derived from geochemical data. *J. Oceanogr.* **2018**, *74*, 453−470.

(15) Pearson, C.; Howard, D.; Moore, C.; Obrist, D. Mercury and trace metal wet deposition across five stations in Alaska: controlling factors, spatial patterns, and source regions. *Atmos. Chem. Phys.* **2019**, *19*, 6913−6929.

(16) Ji, X.; Abakumov, E.; Xie, X. Atmosphere−ocean exchange of heavy metals and polycyclic aromatic hydrocarbons in the Russian Arctic Ocean. *Atmos. Chem. Phys.* **2019**, *19*, 13789−13807.

(17) Leitch, D. R.; Carrie, J.; Lean, D.; Macdonald, R. W.; Stern, G. A.; Wang, F. The delivery of mercury to the Beaufort Sea of the Arctic Ocean by the Mackenzie River. *Sci. Total Environ.* **2007**, *373*, 178−195.

(18) Graydon, J. A.; Emmerton, C. A.; Lesack, L. F. W.; Kelly, E. N. Mercury in the Mackenzie River delta and estuary: Concentrations and fluxes during open-water conditions. *Sci. Total Environ.* **2009**, *407*, 2980−2988.

(19) Lehnherr, I.; St Louis, V. L.; Hintelmann, H.; Kirk, J. L. Methylation of inorganic mercury in polar marine waters. *Nat. Geosci.* **2011**, *4*, 298−302.

(20) Schartup, A. T.; Balcom, P. H.; Soerensen, A. L.; Gosnell, K. J.; Calder, R. S. D.; Mason, R. P.; Sunderland, E. M.; St Louis, V. L. Freshwater discharges drive high levels of methylmercury in Arctic marine biota. *Proc. Natl. Acad. Sci. U.S.A.* **2015**, *112*, 11789−11794.

(21) Wang, F.; Macdonald, R. W.; Armstrong, D. A.; Stern, G. A. Total and methylated mercury in the beaufort sea: The role of local and recent organic remineralization. *Environ. Sci. Technol.* **2012**, *46*, 11821−11828.

(22) Heimbürger, L.-E.; Sonke, J. E.; Cossa, D.; Point, D.; Lagane, C.; Laffont, L.; Galfond, B. T.; Nicolaus, M.; Rabe, B.; van der Loeff, M. R. Shallow methylmercury production in the marginal sea ice zone of the central Arctic Ocean. *Sci. Rep.* **2015**, *5*, 10318.

(23) Baya, P. A.; Gosselin, M.; Lehnherr, I.; St Louis, V. L.; Hintelmann, H. Determination of monomethylmercury and dimethylmercury in the arctic marine boundary layer. *Environ. Sci. Technol.* **2015**, *49*, 223−232.
(24) Point, D.; Sonke, J. E.; Day, R. D.; Roseneau, D. G.; Hobson, K. A.; Vander Pol, S. S.; Moors, A. J.; Pugh, R. S.; Donard, O. F. X.; Becker, P. R. Methylmercury photodegradation influenced by sea-ice cover in Arctic marine ecosystems. *Nat. Geosci.* **2011**, *4*, 188−194.
(25) EPA. U. S. Method 1631, *Revision E: Mercury in Water by Oxidation, Purge and Trap, and Cold Vapor Atomic Fluorescence Spectrometry*; EPA-821-R-02-019, 2002; pp 1−45.
(26) EPA. U. S. Method 1630, *Methyl Mercury in Water by Distillation, Aqueous Ethylation, Purge and Trap, and CVAFS*; EPA-821-R-01-020, 1998; pp 1−49.
(27) EPA. U. S. Method 7473 (SW-846), *Mercury in Solids and Solutions by Thermal Decomposition, Amalgamation, and Atomic Absorption Spectrophotometry*; US Environmental Protection Agency: Washington, DC, 1998; pp 1−17.
(28) Marvin-Dipasquale, M.; Lutz, M.; Krabbenhoft, D.; Aiken, G.; Orem, W.; Hall, B.; Dewild, J.; Brigham, M. *Total Mercury, Methylmercury, Methylmercury Production Potential, and Ancillary Streambed-Sediment and Pore-Water Data for Selected Streams in Oregon*, Wisconsin, and Florida, 2003−04, 2008.
(29) Olund, S. D.; DeWild, J. F.; Olson, M. L.; Tate, M. T. *Methods for the Preparation and Analysis of Solids and Suspended Solids for Total Mercury*; 5-A8; U. S. Geological Survey: Reston, VA, 2004; pp 1−23.
(30) Luengen, A. C.; Fisher, N. S.; Bergamaschi, B. A. Dissolved organic matter reduces algal accumulation of methylmercury. *Environ. Toxicol. Chem.* **2012**, *31*, 1712−1719.
(31) Lee, C.-S.; Fisher, N. S. Methylmercury uptake by diverse marine phytoplankton. *Limnol. Oceanogr.: Methods* **2016**, *61*, 1626−1639.
(32) Chen, M.; Jung, J.; Lee, Y. K.; Hur, J. Surface accumulation of low molecular weight dissolved organic matter in surface waters and horizontal off-shelf spreading of nutrients and humic-like fluorescence in the Chukchi Sea of the Arctic Ocean. *Sci. Total Environ.* **2018**, *639*, 624−632.
(33) Anderson, L. G.; Björk, G.; Holby, O.; Jutterström, S.; Mörth, C. M.; O'Regan, M.; Pearce, C.; Semiletov, I.; Stranne, C.; Stöven, T.; Tanhua, T.; Ulfsbo, A.; Jakobsson, M. Shelf-Basin interaction along the East Siberian Sea. *Ocean Sci.* **2017**, *13*, 349−363.
(34) Chen, M.; Nam, S.-I.; Kim, J.-H.; Kwon, Y.-J.; Hong, S.; Jung, J.; Shin, K.-H.; Hur, J. High abundance of protein-like fluorescence in the Amerasian Basin of Arctic Ocean: Potential implication of a fall phytoplankton bloom. *Sci. Total Environ.* **2017**, *599*−*600*, 355−363.
(35) Lansard, B.; Mucci, A.; Miller, L. A.; Macdonald, R. W.; Gratton, Y. Seasonal variability of water mass distribution in the southeastern Beaufort Sea determined by total alkalinity and δ18O. *J. Geophys. Res.: Planets* **2012**, *117*, 19.
(36) Alkire, M. B.; Falkner, K. K.; Rigor, I.; Steele, M.; Morison, J. The return of Pacific waters to the upper layers of the central Arctic Ocean. *Deep Sea Res., Part I* **2007**, *54*, 1509−1529.
(37) Kirk, J. L.; St Louis, V. L.; Hintelmann, H.; Lehnherr, I.; Else, B.; Poissant, L. Methylated mercury species in marine waters of the Canadian high and sub arctic. *Environ. Sci. Technol.* **2008**, *42*, 8367−8373.
(38) Lindberg, S. E.; Brooks, S.; Lin, C.-J.; Scott, K. J.; Landis, M. S.; Stevens, R. K.; Goodsite, M.; Richter, A. Dynamic oxidation of gaseous mercury in the arctic troposphere at polar sunrise. *Environ. Sci. Technol.* **2002**, *36*, 1245−1256.
(39) Douglas, T. A.; Sturm, M.; Simpson, W. R.; Blum, J. D.; Alvarez-Aviles, L.; Keeler, G. J.; Perovich, D. K.; Biswas, A.; Johnson, K. Influence of snow and ice crystal formation and accumulation on mercury deposition to the arctic. *Environ. Sci. Technol.* **2008**, *42*, 1542−1551.
(40) Dommergue, A.; Larose, C.; Faïn, X.; Clarisse, O.; Foucher, D.; Hintelmann, H.; Schneider, D.; Ferrari, C. P. Deposition of Mercury Species in the Ny-ÅÅlesund Area (79°N) and Their Transfer during Snowmelt. *Environ. Sci. Technol.* **2010**, *44*, 901−907.
(41) DiMento, B. P.; Mason, R. P.; Brooks, S.; Moore, C. The impact of sea ice on the air-sea exchange of mercury in the Arctic Ocean. *Deep Sea Res., Part I* **2019**, *144*, 28−38.
(42) Sommar, J.; Andersson, M. E.; Jacobi, H.-W. Circumpolar measurements of speciated mercury, ozone and carbon monoxide in the boundary layer of the Arctic Ocean. *Atmos. Chem. Phys.* **2010**, *10*, 5031−5045.
(43) Laurier, F. J. G.; Mason, R. P.; Gill, G. A.; Whalin, L. Mercury distributions in the North Pacific Ocean−20 Years of observations. *Mar. Chem.* **2004**, *90*, 3−19.
(44) Agather, A. M.; Bowman, K. L.; Lamborg, C. H.; Hammerschmidt, C. R. Distribution of mercury species in the Western Arctic Ocean (U.S. GEOTRACES GN01). *Mar. Chem.* **2019**, *216*, 103686.
(45) Ardyna, M.; Babin, M.; Gosselin, M.; Devred, E.; Bélanger, S.; Matsuoka, A.; Tremblay, J.-É. Parameterization of vertical chlorophyll a in the Arctic Ocean: impact of the subsurface chlorophyll maximum on regional, seasonal, and annual primary production estimates. *Biogeosciences* **2013**, *10*, 4383−4404.
(46) Fox, A. L.; Hughes, E. A.; Trocine, R. P.; Trefry, J. H.; Schonberg, S. V.; McTigue, N. D.; Lasorsa, B. K.; Konar, B.; Cooper, L. W. Mercury in the northeastern Chukchi Sea: Distribution patterns in seawater and sediments and biomagnification in the benthic food web. *Deep Sea Res., Part II* **2014**, *102*, 56−67.
(47) Hammerschmidt, C. R.; Fitzgerald, W. F. Geochemical Controls on the Production and Distribution of Methylmercury in Near-Shore Marine Sediments. *Environ. Sci. Technol.* **2004**, *38*, 1487−1495.
(48) Teal, L. R.; Parker, R.; Fones, G.; Solana, M. Simultaneous determination of in situ vertical transitions of color, pore-water metals, and visualization of infaunal activity in marine sediments. *Limnol. Oceanogr.: Methods* **2009**, *54*, 1801−1810.
(49) Podar, M.; Gilmour, C. C.; Brandt, C. C.; Soren, A.; Brown, S. D.; Crable, B. R.; Palumbo, A. V.; Somenahally, A. C.; Elias, D. A. Global prevalence and distribution of genes and microorganisms involved in mercury methylation. *Sci. Adv.* **2015**, *1*, No. e1500675.
(50) Monperrus, M.; Tessier, E.; Amouroux, D.; Leynaert, A.; Huonnic, P.; Donard, O. F. X. Mercury methylation, demethylation and reduction rates in coastal and marine surface waters of the Mediterranean Sea. *Mar. Chem.* **2007**, *107*, 49−63.
(51) Hammerschmidt, C. R.; Fitzgerald, W. F. Methylmercury cycling in sediments on the continental shelf of southern New England. *Geochim. Cosmochim. Acta* **2006**, *70*, 918−930.
(52) Sunderland, E. M.; Dalziel, J.; Heyes, A.; Branfireun, B. A.; Krabbenhoft, D. P.; Gobas, F. A. P. C. Response of a macrotidal estuary to changes in anthropogenic mercury loading between 1850 and 2000. *Environ. Sci. Technol.* **2010**, *44*, 1698−1704.
(53) Hammerschmidt, C. R.; Fitzgerald, W. F. Sediment−water exchange of methylmercury determined from shipboard benthic flux chambers. *Mar. Chem.* **2008**, *109*, 86−97.
(54) Hill, V.; Ardyna, M.; Lee, S. H.; Varela, D. E. Decadal trends in phytoplankton production in the Pacific Arctic Region from 1950 to 2012. *Deep Sea Res., Part II* **2018**, *152*, 82−94.
(55) Macdonald, R. W.; Kuzyk, Z. Z. A.; Johannessen, S. C. The vulnerability of Arctic shelf sediments to climate change. *Environ. Technol. Rev.* **2015**, *23*, 461−479.
(56) Armitage, J. M.; Choi, S.-D.; Meyer, T.; Brown, T. N.; Wania, F. Exploring the Role of Shelf Sediments in the Arctic Ocean in Determining the Arctic Contamination Potential of Neutral Organic Contaminants. *Environ. Sci. Technol.* **2013**, *47*, 923−931.
(57) Wang, K.; Munson, K. M.; Beaupré-Laperrière, A.; Mucci, A.; Macdonald, R. W.; Wang, F. Subsurface seawater methylmercury maximum explains biotic mercury concentrations in the Canadian Arctic. *Sci. Rep.* **2018**, *8*, 14465.

https://dx.doi.org/10.1021/acs.est.0c00154
Environ. Sci. Technol. 2020, 54, 9949−9957